Microring and microdisk resonator integrated circuits on a silicon chip

Andrew W. Poon, Linjie Zhou, Chao Li, Nick K. Hon, and Hui Chen

Photonic Device Laboratory, Department of Electronic and Computer Engineering, The Hong Kong University of Science and Technology, Clear Water Bay, The Hong Kong Special Administrative Region, China

Phone: 852-2358-7905; fax: 852-2358-1485; email: eeawpoon@ust.hk

ABSTRACT

We report our latest experimental and numerical work on silicon microresonator passive and electro-optic active devices. On the passive device front, we demonstrate an electrically tunable silicon microring notch filter for converting 3.6-Gbps non-return-to-zero (NRZ) data format to return-to-zero (RZ)-like data format. We show that the converted RZ-like data quality highly depends on the notch filter extinction ratios. On the active device front, we demonstrate a silicon microring modulator using a double-coupled U-bend waveguide as a feedback and a pair of laterally integrated injection-type p-i-n diodes for bias/signal modulation. We show that the microring modulator extinction ratios are electrically controlled by applying a DC-bias across either the feedback-waveguide or the microring while applying a modulation signal across the other p-i-n diode. We also propose silicon microdisk modulators with selectively integrated depletion-type Schottky diodes. Our numerical simulations suggest that the microdisk structures can be advantageous compared with microring structures. We show that electrical rise time on the order of a few ps is feasible using microdisks. We also allude to on-going work on extending the microresonator devices discussed here to building functional silicon optoelectronics integrated circuits.

Keywords: silicon microring, silicon microdisk, silicon microresonators, free-carrier plasma dispersion, silicon photonics, silicon optoelectronics integrated circuits

1. INTRODUCTION

Silicon micrometer-scale ring/disk resonator devices that are fabricated by the mature CMOS-compatible processes have recently attracted considerable interests for optical signal processing applications on photonics chips including in next-generation wavelength-agile optical networks [1], as components for optical interconnects on computer chips [2-4], and as on-chip refractive-index-based label-free biosensors [5, 6]. As an integrated narrowband optical filter, silicon microring resonator-based channel add-drop and notch filters have attained high quality factors $Q \sim 10^5$ [7, 8]. Majority of the demonstrated silicon microresonators are based on conventional circular/racetrack microring [7-11] and microdisk [12, 13] resonators, with alternative devices from our research group using polygonal-shaped [14-17] and spiral-shaped [18, 19] microdisk resonators.

Various silicon microresonator-based switches and modulators using thermooptical [20], mechanical [21], optical [22], and electrooptical (EO) [23-25] mechanisms have been demonstrated. Among these microresonator tuning methods, EO tuning by means of the well-understood free-carrier plasma dispersion effect in silicon [26] offers an appealing combination of beyond-GHz-speed switching, as well as the possibility of electronic control using CMOS circuits on the silicon substrate. Specifically, Xu et al. in their pioneering work [23] demonstrated GHz-speed silicon microring modulators with laterally integrated injection-type p-i-n diodes. Owing to the high-Q resonance sensitivity to minute refractive index changes, the optical rise time at a probe wavelength near resonance can be of order of magnitude shorter than the electrical rise time (carrier transit time), and is not limited by the slow carrier recombination time. Most recently, Xu et al. [24] has further demonstrated their silicon EO microring modulators up to 4-GHz modulation bandwidth. On the industry end, Luxtera Inc. [25] has reported 10-Gbps microring EO modulators using laterally

integrated depletion-type p-n diode. Previously, our research group also demonstrated a silicon microdisk EO modulator using laterally integrated injection-type p-i-n diode with modulation 3-dB bandwidth up to ~500 MHz [27].

Given the impressive track record of silicon microresonator devices, it is thus conceivable that silicon microresonator optoelectronics integrated circuits (OEICs) will be the next major step forward in order to provide optical signal processing functionality beyond any single devices can offer. Indeed, the year 2006 has seen several silicon microresonator OEIC work including modulation of four different WDM channels using cascaded microring modulators [24], and vertical integration of a microdisk add-drop filter with a CMOS transistor in a three-dimensional structure [13].

Here we report our latest experimental and numerical work on three microring and microdisk resonator-based passive and EO active devices recently proposed by our research group. For passive device applications, we exploit our microring resonators for data format conversion. For active device applications, we demonstrate microring carrier injection-type EO modulators with external-feedback control. We also numerically study the use of carrier depletion-type Schottky diodes in microdisk modulators. This paper is divided into the following sections: section 2 on silicon microring filters for data format conversion, section 3 on silicon microring EO modulators with external feedback, section 4 on silicon microdisk EO modulators using selectively integrated depletion-type Schottky diodes, and section 5 concludes the paper with discussion on future work.

2. SILICON MICRORING FILTERS FOR NRZ-TO-PRZ FORMAT CONVERSION

Optical clock recovery is an essential signal processing in optical communications. Current optical networks mostly employ non-return-to-zero (NRZ) data format [28], which does not carry a strong clock component. Thus, clock recovery relies on first converting the NRZ format into return-to-zero (RZ)-like data format, which carries a strong clock component. The RZ-like format is commonly referred to as pseudo-RZ (PRZ) format. Conventional approaches for NRZ-to-PRZ format conversion use linear [29, 30] and nonlinear [31, 32] approaches, as well as integrated optics in the form of asymmetric Mach-Zehnder interferometers (AMZIs) [33]. Most recently [34], we proposed and reported initial demonstration of using silicon microring notch filters for NRZ-to-PRZ format conversion. The method is a linearly optics approach and highly integrated. Here we report further experimental demonstration using electrically tunable microring resonators with laterally integrated p-i-n diodes under various forward biases.

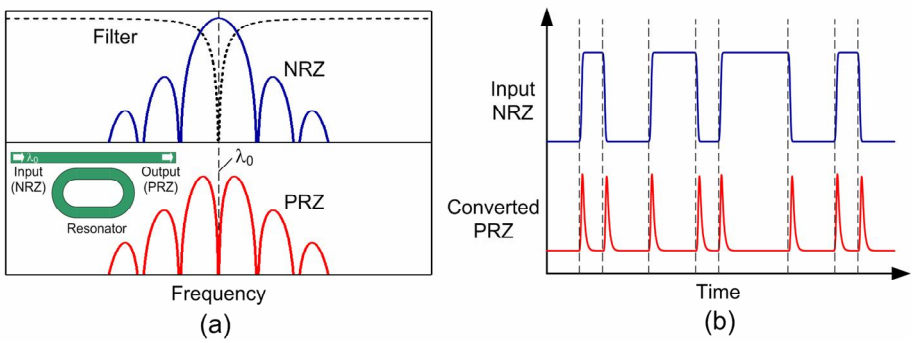

Fig.1. Schematics of the working principle of the microring resonator notch filter-based NRZ-to-PRZ format converter. (a) An input NRZ signal, a notch filter transmission, and the converted PRZ signal in frequency domain. The carrier wavelength of the input NRZ signal is at the microring notch filter wavelength λ_0. Inset: schematic of the waveguide-coupled microring resonator-based notch filter. (b) Schematic waveforms of the input NRZ signal and the converted PRZ signal. The converted PRZ signal pulses follow the transition edges of the input NRZ signal.

Figure 1 illustrates the working principle of the microring resonator notch filter-based NRZ-to-PRZ format converter [34]. Fig. 1(a) shows the schematics of an input NRZ signal, a notch filter transmission, and the converted PRZ signal, all in frequency domain. The inset depicts the schematic of the microring notch filter comprising a single-mode submicrometer waveguide laterally coupled to a racetrack microring resonator. Optical NRZ signal is launched into the

bus waveguide with the carrier wavelength at the microring notch filter wavelength λ_0. After passing through the notch filter, the NRZ signal is converted to a PRZ signal by suppressing the optical carrier frequency components and effectively enhancing the optical clock components in the notch filter transmission. In time domain, the transmission signal appears as discrete PRZ pulses corresponding to the transition edges of the NRZ signal, as shown in Fig. 1(b).

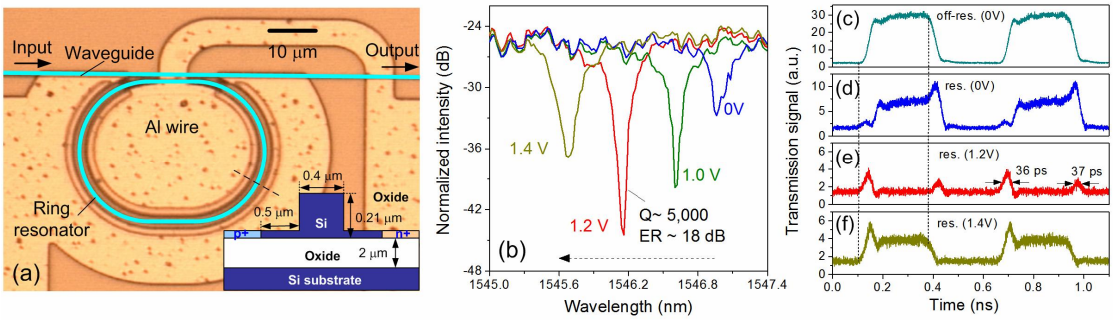

Fig. 2. (a) Optical micrograph of an actively tunable racetrack microring resonator notch filter with laterally integrated p-i-n diode on an SOI substrate. Inset: cross-sectional schematic of the p-i-n diode. (b) Measured TE-polarized throughput-port spectrum upon various forward biases. (c) – (f) Measured transmission of a 3.6-Gbps NRZ signal at (c) an off-resonance carrier wavelength (1546 nm, cyan line), (d) an on-resonance carrier wavelength under 0-V forward bias (1546.9 nm, blue line), (e) an on-resonance carrier wavelength under 1.2-V forward bias (1546.15 nm, red line), and (f) an on-resonance carrier wavelength under 1.4-V forward bias (1545.68 nm, yellow line).

Figure 2(a) shows an optical micrograph of our fabricated racetrack microring resonator-based notch filter with laterally integrated p-i-n diode surrounding most of the microring on a silicon-on-insulator (SOI) substrate. The fabrication employs i-line optical lithography and dry etching as in our previous work [27]. The integrated diode enables active EO tuning in order to match the notch filter wavelength with the signal carrier wavelength. The racetrack arc radius is 25 μm and the straight interaction length is 10 μm. Inset shows the cross-sectional schematic of the laterally integrated p-i-n diode. The rib waveguide in the intrinsic region has a width of 0.4 μm, a height of 0.21 μm, and an etched depth of 0.18 μm. The p^+-doped ($2x10^{19}$ cm^{-3}) and n^+-doped ($1x10^{20}$ cm^{-3}) regions are positioned in the slab layer, with ~0.5-μm separations from the waveguide sidewalls.

Figure 2(b) shows the measured TE-polarized (electric field in the device plane) transmission spectra with the p-i-n diode forward biased at 0 V, 1.0 V, 1.2 V, and 1.4 V. Under 0-V bias, the transmission dip (Q ~ 5,000) only exhibits an extinction ratio (ER) of ~6 dB. As the diode is gradually forward biased (beyond the threshold voltage of ~0.75 V), the carrier-induced resonance wavelength blueshift and the ER increases with forward biases until reaching an optimum at ~18 dB upon a 1.2-V bias, suggesting a transition from over-coupling to critical coupling regimes.

Figures 2(c) – 2(f) show the measured 3.6-Gbps NRZ signal transmission waveforms at an off-resonance wavelength (0-V bias) and at on-resonance wavelengths upon forward biases at 0 V, 1.2 V, and 1.4 V. The off-resonance waveform largely follows the input NRZ signal (except for the ripples observed in the optical waveform). The optical signal displays a rise time of ~30 ps and a fall time of ~35 ps. The on-resonance waveform upon 1.2-V bias displays PRZ pulses following the transition edges with pulse widths of ~36 ps and a peak extinction ratio of ~6 dB for the rising edge pulses. The shorter NRZ signal rise time gives rise to higher PRZ pulse amplitudes. Whereas, the on-resonance waveform upon 0-V (1.4-V) bias displays a distorted NRZ signal, with an overshoot at the signal falling (rising) edge and a dip followed with a slight peak at the signal rising (falling) edge. We note that the relatively low ERs (< 10 dB) upon 0-V and 1.4-V biases render less optical carrier suppression and thereby less pronounced clock components.

3. SILICON MICRORING ELECTRO-OPTIC MODULATORS WITH EXTERNAL FEEDBACK

In this section, we extend our actively tunable silicon microring notch filter work to an actively reconfigurable EO modulator. We propose and initially demonstrate a silicon microring EO modulator that can be actively tuned by means of an external feedback. The concept is based on our previous work on silicon microring notch filter comprising a microring that is double-coupled to a U-bend waveguide [35]. Here as a modulator, both the microring and the feedback

waveguide are laterally integrated with p-i-n diodes, allowing biasing and signal modulation to be separately applied across the two sets of p-i-n diodes. The biasing electrically tunes the resonance wavelength and ER.

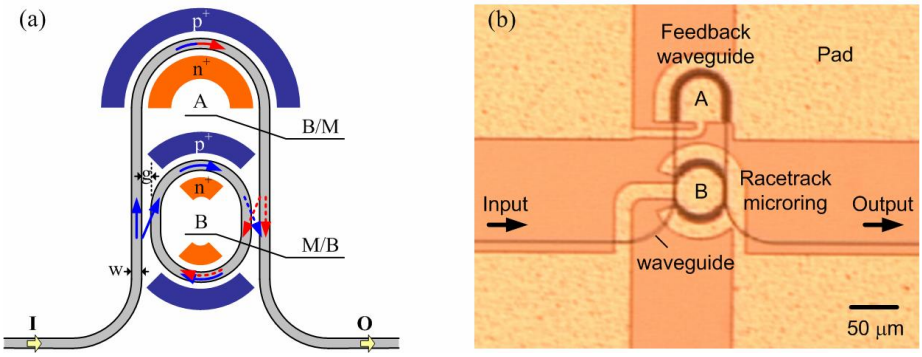

Fig. 3. (a) Schematic of the proposed silicon microring EO modulator with external-feedback control using two terminals of lateral integrated p-i-n diodes. The heavily-doped n^+- and p^+-type regions are laterally integrated across the U-bend waveguide and two arcs of the microring. B: Biasing; M: Modulation. I: Input; O: Output. w: waveguide width; g: gap separation between the waveguide and the coupled microring. (b) Top-view optical micrograph of the fabricated microring modulator with external feedback in a thin SOI substrate.

Figure 3(a) depicts a schematic and the working principle of our proposed microring modulator with external feedback. The modulator comprises a racetrack microring resonator that is input- and output-coupled to a single-mode U-bend waveguide. The arrows indicate the lightwave propagation and coupling in the feedback-coupled microring resonator. One p-i-n diode (node A) is laterally integrated with the U-bend feedback-waveguide and two other p-i-n diodes (node B) are laterally integrated across two arcs of the microring resonator. We note that both nodes A and B can be employed for biasing and signal modulation. For example, by DC-biasing node A, we electro-optically tune the phase-matching condition of the feedback-coupled microring resonator, and thereby tuning the modulator operating resonance wavelength and ER.

We again employ standard silicon nanofabrication processes as in our previous work [27]. Fig. 3(b) shows the top-view optical micrograph of the fabricated modulator. The racetrack ring dimensions and the p-i-n diode cross sections are the same as in Sec. 2. The p-i-n diode integrated with the U-bend waveguide is 130-μm-long. Whereas, the p-i-n diodes integrated with the microring arcs are 117-μm-long.

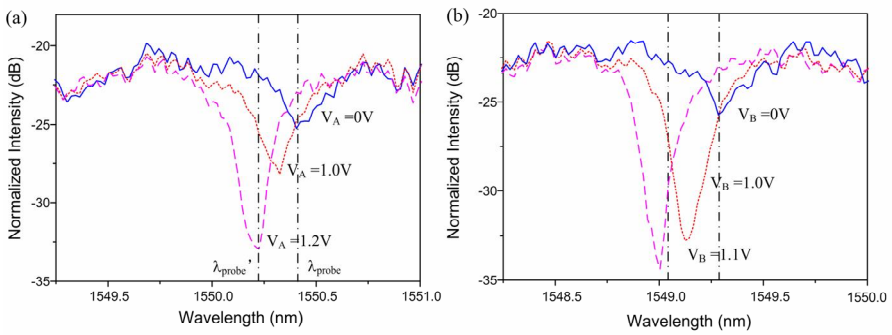

Fig. 4. (a) Measured TE-polarized transmission spectra under various DC-bias voltages of $V_A = 0$ V (solid line), 1.0 V (dotted line), and 1.2 V (dashed line). (b) Measured TE-polarized transmission spectra under various DC-bias voltages of $V_B = 0$ V (solid line), 1.0 V (dotted line), and 1.1 V (dashed line).

Figure 4(a) shows the measured TE-polarized transmission spectra under various DC forward biases only across node A (V_A) of 0 V, 1.0 V, and 1.2 V. Upon $V_A = 0$ V, we observe an ER of ~4 dB. As we forward-bias node *A*, the resonance wavelength gradually blueshifts with an enhanced ER until reaching the maximum ER of ~12 dB upon $V_A = 1.2$ V. We attribute this resonance enhancement to critical coupling between the microring resonator and the feedback waveguide [35]. Fig. 4(b) shows the measured TE-polarized transmission spectra under various DC forward biases only across node

B (V_B) of 0 V, 1.0 V, and 1.1 V. Similarly, we observe an ER of ~13 dB upon V_B = 1.1 V, an enhancement compared with that of ~4 dB upon V_B = 0 V.

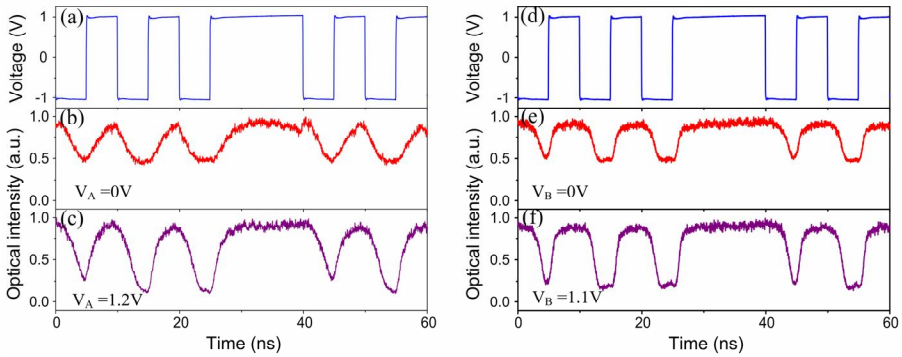

Fig. 5. (a) Electrical input data stream with ±1-V signal levels applied across node *B*. (b) and (c) Measured 200-Mbps NRZ optical waveforms at a probe wavelength in the vicinity of a resonance under V_A = 0 V, and V_A = 1.2 V. (d) Electrical input data stream with ±1-V signal levels applied across node *A*. (e) and (f) Measured 200-Mbps NRZ optical waveforms at a probe wavelength in the vicinity of a resonance under V_B = 0 V, and V_B = 1.1 V.

In order to examine the modulator response, we apply a 200-Mbps NRZ electrical driving signal with ±1-V signal levels at node *B*, as shown in Fig. 5(a), while launching a probe wavelength in the vicinity of the resonance. Fig. 5(b) shows the modulated optical waveform for V_A = 0 V. We observe only ~55% modulation depth which is consistent with the ER of ~4 dB. Fig. 5(c) shows the modulated optical waveform for V_A = 1.2 V. The modulation depth is improved to ~90% which is consistent with the enhanced ER of ~12 dB.

Similarly, we also forward-bias node *B* (V_B) and modulate node *A* by applying the same electrical driving signal, as shown in Fig. 5(d). Figs. 5(e) and 5(f) show the modulated optical waveforms for V_B = 0 V and V_B = 1.1 V. We observe that the modulation depth improves from ~50% (V_B = 0 V) to ~85% (V_B = 1.1 V). We remark that the optical waveforms from node A modulation exhibit shorter rise and fall times than those from node B modulation (see Figs. 5(b) and 5(c)). We attribute this improvement to relatively less free-carriers diffusion escape near the two ends of the long diode-integrated U-bend waveguide. Thus, most of the free carriers can be swept out upon reverse bias. In contrast, modulating the relatively short arcs of the partially wrapped microring allows more carriers to escape by diffusion, and thereby slowing down the modulation response [23, 24].

4. SILICON MICRODISK ELECTRO-OPTIC MODULATORS USING SELECTIVELY INTEGRATED DEPLETION-TYPE SCHOTTKY DIODES

In this section, we numerically examine our recently proposed class of silicon EO modulators using microdisk resonators with selectively integrated depletion-type Schottky diodes [36]. Compared with microring resonators, microdisk resonators applied as EO modulators offer three key advantages. On the optics front, microdisk resonators have no inner sidewall scattering loss, and thereby whispering-gallery modes (WGMs) that graze along the microdisk rim are of intrinsically higher Q than the microring resonances. On the fabrication end, microdisk structures eliminate the undesirable polarization-mode mixing and cavity losses due to fabrication error induced microring waveguide width non-uniformity. On the electrical front, our numerical simulation suggests that depletion-type EO modulators using microdisk structures have higher modulation bandwidth than microring structures.

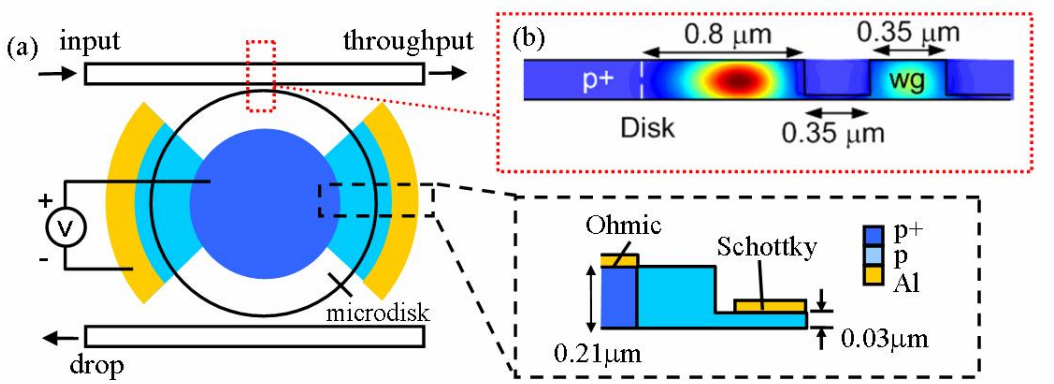

Fig. 6 (a) Schematic of a silicon microdisk EO modulator with selectively integrated depletion-type Schottky diode. Inset: schematic cross-section of the Schottky diode. Al: aluminum. (b) FDTD-simulated TE-polarized mode-field profiles of a 1st-order mode at the coupling region. Our three-dimensional FDTD simulations assume a side-coupled waveguide width of 0.35 μm, a coupling gap of 0.35 μm, and a microdisk diameter of 5 μm. wg: waveguide.

Fig. 6(a) shows the schematic of our proposed design [36]. The inset shows the Schottky diode cross-section schematic. We adopt Schottky diode instead of the conventional p-n diode because metal-semiconductor junction has less parasitic series resistance than p-n junction. Moreover, fewer processing steps are imposed as Schottky contact can be obtained by depositing a metal film on the silicon wafer while defining the electrical contact patterns. The Schottky contact is formed on the slab region immediately outside the microdisk rim. The microdisk rim is p-typed slightly doped in order to provide the necessary concentration of depleted free-carriers upon reverse biasing the diode. As the diode is reverse-biased, the majority carriers (h^+) in the microdisk rim region are swept out by the internal electric field. When the diode is no longer biased, the majority carriers are swept back to neutralize the charges in the depletion region. Thus, in each modulation cycle, the free-carriers drift under the applied reverse bias or the internal electric field set by the depleted acceptor ions. The absence of the slow injection carriers (transport by diffusion) potentially offers high-speed optical switching. The microdisk central region is p-type highly doped in order to define the ohmic contact.

In selectively embedding the Schottky diode, the microdisk p^+-doped central region should be wide enough in order to preferentially suppress the higher-order WGMs, and in principle, only retain the 1st-order WGM [37]. Whereas the microdisk rim should be narrow enough in order to reduce the parasitic resistance. Here we define the central doped region relative radius r as the ratio of the p^+-doped central region radius to the microdisk radius. Our simulations of a 5-μm-diameter microdisk suggest that we can adopt $r = 0.68$ (disk rim width = 0.8 μm) in order to preferentially suppress the higher-order WGMs while retaining only the 1st- order WGM. Fig. 6(b) shows the three-dimensional FDTD-simulated cross-sectional mode-field profiles at the coupling region of a 1st-order WGM.

Here we calculate the carrier concentration variations in the microdisk rim region using a two-dimensional semiconductor device numerical simulation tool MEDICI. We then compute the carrier-induced refractive index change Δn using the free-carrier plasma dispersion formulae in silicon according to Soref and Bennett [26]. Fig. 7(a) shows the calculated Δn using 8 V reverse bias across the metal-rim separation. We see that the smaller is the separation (thereby the larger is the applied field), the larger is the Δn. As a rule-of-thumb, in order to redshift a $Q \sim 10^4$ resonance mode by about a linewidth, we need a refractive index change of $\sim 10^{-4}$. We choose the metal-rim separation to be 0.4 μm which provides sufficient Δn without imposing significant spatial overlap with the WGM field (see Fig. 6(b)). Fig. 7(b) shows the calculated Δn at various rim p-doping concentrations (under 8-V reverse bias and 0.4-μm metal-rim separation). We observe the maximum Δn at rim p-doping concentration of $\sim 5 \times 10^{16}$ cm^{-3}.

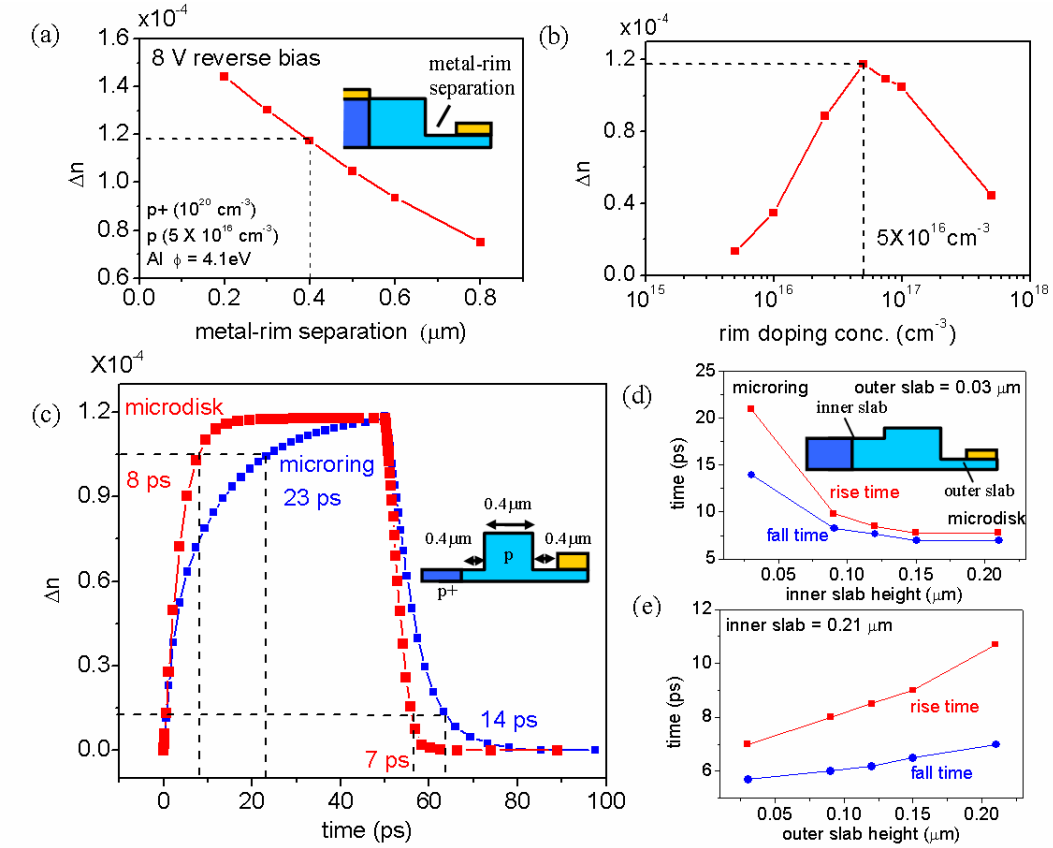

Fig. 7 (a) Calculated free-carrier induced refractive index change Δn as a function of the metal-rim separation upon 8-V reverse bias. Inset illustrates the metal-rim separation. (b) Calculated Δn as a function of p-doping concentration in the microdisk rim. (c) Calculated Δn temporal response in the microdisk rim region (red) and in a (microring) waveguide (blue) from 0 V to -8 V and back to 0 V. Inset: schematic cross-section of a (microring) waveguide with a laterally integrated Schottky diode of the same ohmic-to-Schottky separation as in the microdisk. (d) Calculated Δn rise and fall times as a function of the inner slab height (with fixed outer slab height at 0.03 μm). Inset illustrates the inner and outer slab heights. (e) Calculated Δn rise and fall times as a function of the outer slab height (with fixed inner slab height at 0.21 μm).

Fig. 7(c) shows the calculated Δn temporal response of a microdisk rim and a (microring) waveguide structure of the same ohmic-to-Schottky separation of 1.2 μm. Inset shows the waveguide cross section. The diode is revered-biased from 0 V to -8 V and back to 0 V. The rise and fall times (~8 ps) of the microdisk are shorter than those of the waveguide structure (23 ps – 14 ps). The electrical bandwidth of the Schottky diode is thus ~40 GHz. We attribute the faster switching times of the microdisk than of the (microring) waveguide to the relatively low resistance provided by the larger interface between the p^+-doped central region and the microdisk rim region.

In order to support the above argument, Fig. 7(d) shows the calculated Δn rise and fall times at various inner slab heights (fixed outer slab height at 0.03 μm). Inset illustrates the inner and outer slab heights. An inner slab height of 0.21 μm corresponds to the microdisk structure, whereas an inner slab height of 0.03 μm corresponds to the (microring) waveguide structure. The increase in the inner slab height increases the interface between the microdisk rim region and the p^+-doped region, and thereby reduces the junction resistance. Fig. 7(c) shows the calculated Δn rise and fall times at various outer slab heights. The effect of changing the outer slab height is less significant compared with varying the inner slab height because free-carriers (h^+) are swept in and out between the p^+-doped central region and the p-doped rim region (but not via the Schottky contact).

It should be emphasized that the bandwidth of a microresonator-based modulator is fundamentally limited by the photon cavity lifetime τ as the resonance mode needs time to build up and decay [36]. For a mode with Q ~ 10^4, the decay time

can be estimated using the relation $Q = \omega\tau$, where ω is the resonance frequency. The estimated cavity lifetime is on the order of 20 ps. Thus, the optical bandwidth of the proposed microdisk modulator can reach around 20 GHz ($0.35/\tau$) and is fundamentally limited by the cavity lifetime.

5. CONCLUSIONS AND FUTURE WORK

In summary, we reported our recent work on three silicon microresonator filters and modulators which can be relevant building blocks to emergent application-specific OEICs on silicon chips. We experimentally investigated NRZ-to-PRZ format conversion using electrically tunable microring resonator-based notch filters with laterally integrated p-i-n diodes. We showed that high-extinction-ratio resonances with critical coupling are essential in order to obtain pronounced converted PRZ signals. We also experimentally demonstrated a silicon microring carrier-injection-type modulator with a double-coupled U-bend waveguide as an external feedback. By applying a DC-bias either across the feedback waveguide or the microring, we demonstrated resonance tuning with controlled extinction ratio exceeding 10 dB at an optimum bias voltage of the order of 1 V. Our initial experiments also suggested better modulator response from modulating the long U-bend feedback-waveguide than from modulating the short arcs of the microring. Lastly, we numerically examined a silicon microdisk resonator-based EO modulators using selectively embedded depletion-type Schottky diode that enables higher modulation bandwidths than conventional injection-type diode. We showed that microdisk structures offer faster switching times (~8 ps) than microring structures. Our analysis further suggested that our proposed device is fundamentally limited by the cavity lifetime which limits the optical bandwidth to around 20 GHz.

In our on-going work, we seek to implement a silicon OEIC chip for clock recovery from high-data-rate NRZ signals using an integrated microring notch filter for NRZ-to-PRZ format conversion and a microring/microdisk EO modulator (injection-type or depletion-type) driven by an external optoelectronic phase-locked loop as a phase comparator in order to temporally gate the converted PRZ pulses. We envision that this kind of clock-recovery OEIC can find applications in high-data-rate signal processing in fiber-optic networks [1], and also in optical interconnects for Ultra-Short-Reach applications in computer chips [3].

ACKNOWLEDGEMENTS

This study was substantially supported by grants from the Research Grants Council of the Hong Kong Special Administrative Region, China (projects HKUST6112/03E, HKUST6254/04E, & 618505).

REFERENCES

[1] P. Herve, and S. Ovadia, "Optical technologies for enterprise networks," *Intel. Technol. J.* **8**, 73 (2004).
[2] D. A. B. Miller, "Rationale and challenges for optical interconnects to electronic chips," *Proc. IEEE* **88**, 728 (2000).
[3] E. Mohammed, A. Alduino, T. Thomas, H. Braunisch, D. Lu, J. Heck, A. Liu, I. Young, B. Barnett, G. Vandentop, and R. Mooney, "Optical interconnect system integration for ultra short reach applications," *Intel. Technol. J.* **8**, 115 (2004).
[4] L. Pavesi and G. Guillot, Optical Interconnects: *The Silicon Approach (Springer Series in Optical Sciences)*. New York: Springer, 2006.
[5] E. Krioukov, D. J. W. Klunder, A. Driessen, J. Greve, and C. Otto, "Sensor based on an integrated optical microcavity," *Opt. Lett.* **27**, 512 (2002).
[6] N. M. Jokerst, M. A. Brooke, S. Cho, M. Thomas, J. Lillie, D. Kim, S. Ralph, and K. Dennis, "Integrated planar lightwave bio/chem. OEIC sensors on Si CMOS circuits," *Proc. SPIE* **5730**, 226 (2005).
[7] J. Niehusmann, A. Vörckel, P. H. Bolivar, T. Wahlbrink, W. Henschel, and H. Kurz, "Ultrahigh-quality-factor silicon-on-insulator microring resonator," *Opt. Lett.* **29**, 2861 (2004).
[8] I. Kiyat, A. Aydinli, and N. Dagli, "High-Q silicon-on-insulator optical rib waveguide racetrack resonators," *Opt. Express* **13**, 1900 (2005).
[9] F. Xia, L. Sekaric, M. O'Boyle, and Y. Vlasov, "Coupled resonator optical waveguides based on silicon-on-insulator photonic wires," *Appl. Phy. Lett.* **89**, 041122 (2006).
[10] Q. Xu, S. Sandhu, M. L. Povinelli, J. Shakya, S. Fan, and M. Lipson, "Experimental realization of an on-chip all-optical analogue to electromagnetically induced transparency," *Phy. Rev. Lett.* **96**, 123901 (2006).

[11] M. A. Popović, T. Barwicz, M. R. Watts, P. T. Rakich, L. Socci, E. P. Ippen, F. X. Kärtner, and H. I. Smith, "Multistage high-order microring-resonator add-drop filters," *Opt. Lett.* **31**, 2571 (2006).
[12] A. Kazmierczak, M. Brière, E. Drouard, P. Bontoux, P. Rojo-Romeo, I. O'Connor, X. Letartre, F. Gaffiot, R. Orobtchouk, and T. Benyattou, "Design, simulation, and characterization of a passive optical add-drop filter in silicon-on-insulator technology," *IEEE Photon. Technol. Lett.* **17**, 1447 (2005)
[13] P. Koonath, T. Indukuri, and B. Jalali, "Monolithic 3-D silicon photonics," *J. Lightwave Technol.* **24**, 1796, (2006).
[14] N. Ma, C. Li, and A W. Poon, "Laterally coupled hexagonal micro-pillar resonator add-drop filters in silicon nitride," *IEEE Photon. Technol. Lett.* **16**, 2487 (2004).
[15] C. Li, N. Ma, and A. W. Poon, "Waveguide-coupled octagonal microdisk channel add-drop filters," *Opt. Lett.* **29**, 471 (2004).
[16] C. Li and A. W. Poon, "Experimental demonstration of waveguide-coupled round-cornered octagonal microresonators in silicon nitride", *Opt. Lett.* **30**, 546 (2005).
[17] C. Li, L. Zhou, S. Zheng, and A. W. Poon, "Silicon polygonal microdisk resonators," *IEEE J. Sel. Topics Quantum Electron. (special issue on silicon photonics)* **12**, 1438 (2006).
[18] J. Y. Lee and A. W. Poon, "Spiral micropillar resonator-based unidirectional channel drop filters," in *Proc. 8th International Conference on Transparent Optical Networks*, Nottingham, UK, conference proceedings, **1**, pp. 62-65, 2006.
[19] J. Y. Lee and A. W. Poon, "Spiral-shaped microdisk resonator-based channel drop filters on a silicon nitride chip," in *proceedings of IEEE 3rd International Conference on Group IV Photonics*, Ottawa, ON, Canada, pp. 19-21, 2006.
[20] I. Kiyat, A. Aydinli, and N. Dagli, "Low-power thermooptical tuning of SOI resonator switch," *IEEE Photon. Technol. Lett.* **18**, 364 (2006).
[21] G. N. Nielson, D. Seneviratne, F. Lopez-Royo, P. T. Rakich, Y. Avrahami, M. R. Watts, H. A. Haus, H. L. Tuller, and G. Barbastathis, "Integrated wavelength-selective optical MEMS switching using ring resonator filters," *IEEE Photon. Technol. Lett.* **17**, 1190 (2005).
[22] V. R. Almeida, C. A. Barrios, R. R. Panepucci, and M. Lipson, "All-optical control of light on a silicon chip," *Nature* **431**, 1081 (2004).
[23] Q. Xu, B. Shmidt, S. Pradhan, and M. Lipson, "Micrometre-scale silicon electro-optic modulator," *Nature* **435**, 325 (2005).
[24] Q. Xu, B. Schmidt, J. Shakya, and M. Lipson, "Cascaded silicon micro-ring modulators for WDM optical interconnection," *Opt. Express* **14**, 9430 (2006).
[25] C. Gunn, "CMOS photonics technology platform", invited paper 6125-01, SPIE Photonics West, *SPIE Proceedings vol. 6125 on Silicon Photonics*, San Jose, CA, 25 Jan 2006.
[26] R. A. Soref and B. R. Bennett, "Electrooptical effects in silicon," *IEEE J. Quantum Electron.* **QE-23**, 123 (1987).
[27] L. Zhou and A. W. Poon, "Silicon electro-optic modulators using p-i-n diodes embedded 10-micron-diameter microdisk resonators," *Opt. Express* **14**, 6851 (2006).
[28] G. P. Agrawal: *Fiber-optic communication systems (3rd edition)*. New York: Wiley, 2004.
[29] X. Li, C. Kim, and G. Li, "All-optical passive clock extraction of 40 Gbit/s NRZ data using narrow-band filtering," *Opt. Express* **12**, 3196 (2004).
[30] C.-H. Lee and H. K. Lee, "Passive all-optical clock signal extractor for non-return-to-zero signals," *Electron. Lett.* **34**, 295 (1998).
[31] A. Reale, P. Lugli, and S. Betti, "Format conversion of optical data using four-wave mixing in semiconductor optical amplifiers," *IEEE J. Sel. Topics Quantum Electron.* **7**, 703 (2001).
[32] J. Slovak, C. Bornholdt, J. Kreissl, S. Bauer, M. Biletzke, M. Schlak, and B. Sartorius, "Bit rate and wavelength transparent all-optical clock recovery scheme for NRZ-coded PRBS signals," *IEEE Photon. Technol. Lett.* **18**, 844 (2006).
[33] J. Yu, G. K. Chang, J. Barry, and Y. Su, "40 Gbit/s signal format conversion from NRZ to RZ using a Mach-Zehnder delay interferometer," *Opt. Communications* **248**, 419 (2004).
[34] L. Zhou, H. Chen and A. W. Poon, "NRZ-to-PRZ format converters using narrowband 10-GHz-bandwidth microresonator-based notch filters," manuscript submitted to Conference on Lasers Electro-Optics, Baltimore, Maryland, May 7-12, 2007.
[35] L. Zhou and A. W. Poon, "Silicon electro-optics switches using microring resonators with phase-tunable feedback," in *proceedings of IEEE/LEOS 3rd International Conference on Group IV Photonics*, Ottawa, Canada, Sep. 13-15, 2006.

[36] N. K. Hon, L. Zhou and A.W. Poon, "Silicon depletion-type microdisk electro-optic modulators using selectively integrated Schottky diodes" manuscript submitted to Conference on Lasers Electro-Optics, Baltimore, Maryland, May 7-12, 2007.
[37] L. Zhou and A. W. Poon, "Silicon-on-insulator tunable waveguide-coupled microdisk resonators with selectively integrated p-i-n diodes" in *proceedings of Conference on Lasers and Electro-Optics*, Baltimore, Maryland, May 22-27 2005.